Impedance of a Small Electrically Isolated Area of the Muscle Cell Surface

A. STRICKHOLM

From the Department of Physiology, University of Chicago. Dr. Strickholm's present address is the Physiological Institute, University of Uppsala, Uppsala, Sweden

ABSTRACT A method has been developed permitting measurement of membrane impedance and current, as a function of transmembrane potential, at small, electrically isolated regions of the muscle cell surface without microelectrode impalement. The frequency dependence of the muscle cell membrane capacity found earlier by other methods has been confirmed. The average capacity is 3.5 $\mu f/cm^2$ with a phase angle of 71° at 5 kilocycles. The internal phase angle of the complex impedance plot of whole muscle probably does not result from a distribution of fiber diameters and membrane capacities, since it also appears in the present experiments where measurements are confined to a small region of a single fiber.

INTRODUCTION

Impedance measurements on whole muscle have suggested that the resting membrane cannot adequately be represented by pure resistive and capacitive structures, but requires non-linear and frequency-dependent elements (Cole and Curtis, 1936; Bozler and Cole, 1935; Cole, 1933, 1932). The present experiments confirm the frequency dependence of the capacity which has been measured by a microelectrode technique obviating the need for cell impalement. This paper describes the method and measurements of resting membrane capacity.

A smooth tipped, liquid-filled micropipette (several microns tip diameter) (Fig. 1) is placed against a muscle in such a way that the cell surface under it is electrically isolated except for a leakage resistance path (R_1) between tip and cell (Fig. 2). This leakage path may derive in part from microfibrils (Robertson, 1956) separating the pipette from the resistive membrane. Placed against plastic films the pipettes show nearly perfect sealing with leakage resistance over 10^8 ohms. Previous use of electrodes to confine electrically a small surface region differed from these experiments in the pipette manufacture (Huxley and Taylor, 1958; Steinman, 1937; Gelfan, 1930; Gelfan and Gerard, 1930; Pratt, 1930; Pratt and Eisenberger, 1919; Taylor, 1925).

Ordinarily the leakage resistance is less than that of the delimited membrane area during rest or excitation. The local surface voltage at the pipette tip with respect to ground may be changed by passing current through the pipette and the resistive paths from pipette tip and muscle surface to ground. Membrane-generated currents passing through the leakage resistance are measured as a small change in the applied surface voltage, and these currents flowing

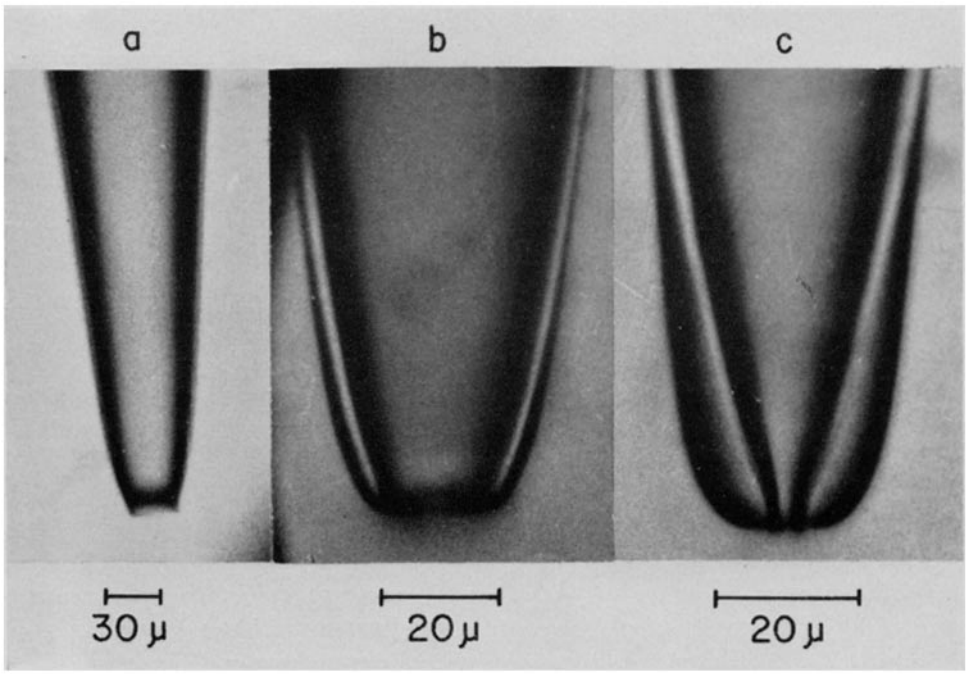

FIGURE 1. Production of smooth tipped micropipettes. (*a*) Pipette tip immediately after pulling showing separation at first undulation. Tip too sharp to be used. (*b*) Heat flashing tip of (*a*) for a few seconds. Tip adequate for use. (*c*) Further heat flashing of tip. Tip not satisfactory for use since the leakage resistance path will be too long.

across the small surface area examined, change the voltage of the subjacent cell interior but slightly (Huxley and Taylor, 1958). Consequently, the region may be hyperpolarized or depolarized without gross changes in the applied transmembrane potential resulting when membrane currents flow.

Voltages produced by an alternating current signal passed through the impedances of the pipette and circuit pathways to ground can be measured, and thus impedance can be measured simultaneously with membrane currents initiated by depolarization. Preliminary experiments relating membrane current and impedance as functions of transmembrane potential have been described (Strickholm, 1960).

MATERIALS AND METHODS

A. *Materials*

The frog sartorius muscle (*Rana pipiens*) has been used almost exclusively, and at a temperature of 5–10°C, usually 7°. Ringer solution contained NaCl 111 mM, KCl 2 mM, $CaCl_2$ 1 mM, $NaHCO_3$ 2.4 mM, NaH_2PO_4 0.008 mM, and sucrose 22.8 mM.

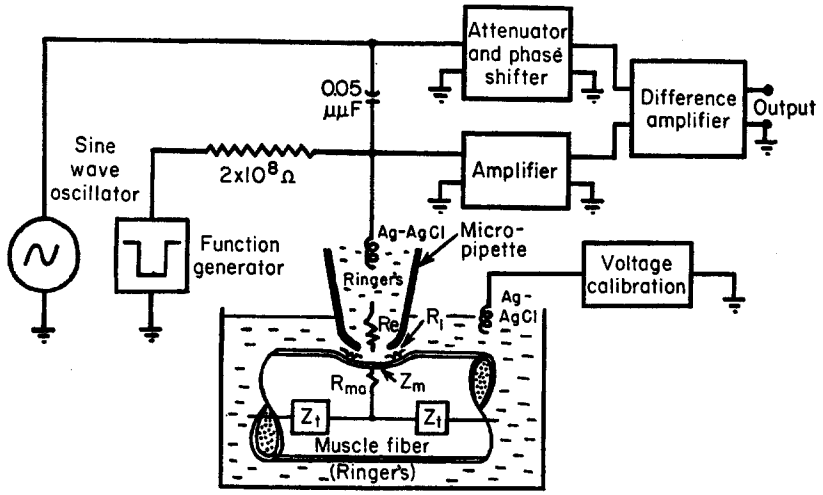

FIGURE 2. Method for local excitation and impedance recording. R_e, pipette resistance, R_l leakage resistance, R_{ma}, membrane access resistance, Z_m, membrane impedance, Z_t, transmission line impedance of muscle.

B. *Micropipette Electrodes*

Smooth tipped pipettes are prepared from 1 to 2 mm diameter melting point tubing by vertical pulling, in a nichrome wire heating coil of a few turns, with a 50 to 250 gm weight. Soft glass is preferable but adequate electrodes have been made of quartz.

The tubing, reduced in diameter to a few tenths of a millimeter, is first tapered rapidly in the upper electrode portion, since tip tapers of large solid angle have lower resistance and minimize difficulties with distributed capacitance. The region where the upper taper ends at the smaller diameter is then heated and pulled slowly, the coil temperature being adjusted so elongation is just perceptible. After a few minutes the tubing suddenly separates. The tip, broken off squarely (Fig. 1 *a*), will usually show microscopic undulations (Plateau, 1917), and will vary from a few to 50 microns, depending upon the glass, pulling rate, and the heating coil dimensions. Softer glass, under low tension, produces larger tips. The tip is then held in the coil or close to a hot wire, whereupon, in a few seconds, it softens and is smoothed by surface tension (Fig. 1 *b*). This also thickens the wall increasing strength and reducing capacitance. Smoothing should be done immediately, since adherent dust makes it impossible to obtain flat tips. The pipettes are then stored or filled either by forcing solution into the large end with a syringe or by aspiration. The latter is preferable, since micro-

splinters of glass are usually washed out by liquid moving upward from the tip. If the electrode is used vertically such particles often settle, protrude, and tear the cell, making local excitation impossible. One must be careful not prematurely to ascribe local inexcitability to deteriorated muscle.

C. *Instrumentation*

The method for changing local surface voltage and for A.C. impedance monitoring is diagrammed in Fig. 2.

Applying a constant rectangular voltage pulse to a 200 megohm resistor, of nine

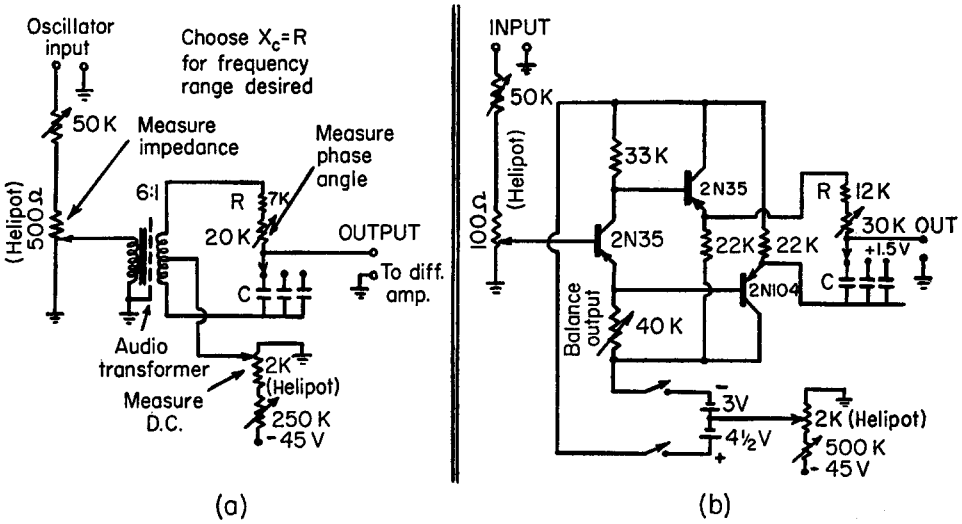

FIGURE 3. Impedance measuring and phase shifting circuits. (*a*) Transformer circuit. (*b*) Transistor circuit.

22 megohm resistors in series to minimize capacitive shunting, delivers constant current through the pipette since the pipette and leakage resistances are usually 1 to 2 megohms each.

Alternating current for impedance measurement comes from a sine wave oscillator coupled to the pipette by a variable 0.01 to 0.05 $\mu\mu$f condenser which is simply an adjustable screw, placed several centimeters from the input grid, and whose impedance, at the frequencies used up to 25 kc, is high relative to the micropipette and leakage resistance. This sytem, therefore, also generates constant current. The use of a small condenser maintains a constant phase angle of 90° for the injected current with respect to the oscillator voltage over the frequencies used. The alternative of injecting A.C. through a high resistance is undesirable as phase shifts occur at higher frequencies. The amplifier A.C. voltage recorded may be calibrated to read impedance directly. This follows from the vector relationship $V = iZ$ where the current, i, is a constant.

This impedance method permits continuous monitoring of electrode resistance and integrity, indicates contact of electrode with tissue, and gives information about diffusion processes at the tip such as occur when the medium is changed (Strickholm, 1957). The method loads the amplifier with little input capacitance and introduces no grid current.

The impedance signal is measured by comparison or nulling in a difference amplifier. The appropriate A.C. comparison signal is obtained by feeding the oscillator output through a calibrated attenuator reading impedance or voltage, and then through a phase-shifting network calibrated to read phase angle. Two impedance measuring circuits have been used. The first (Fig. 3 *a*) uses a transformer and requires

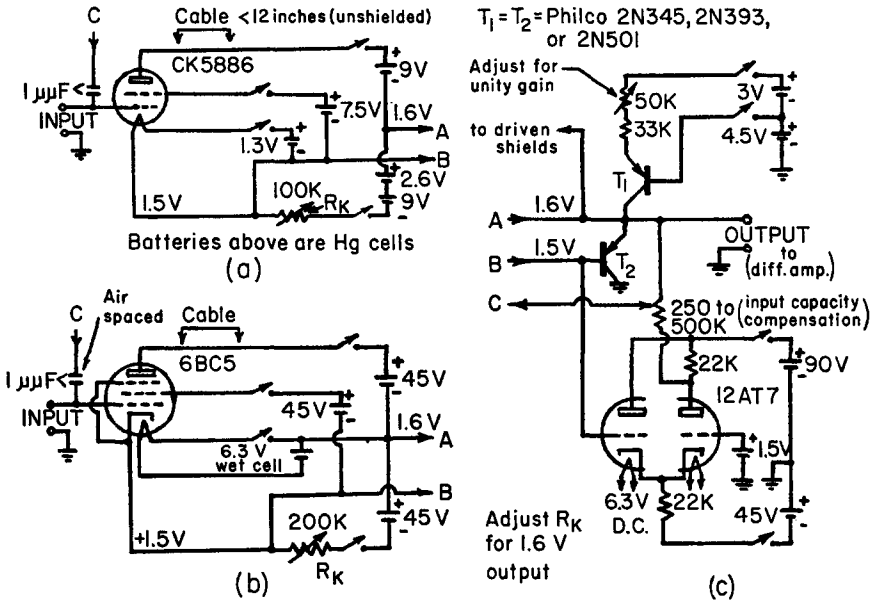

FIGURE 4. Headstage input amplifier. (*a*) Electrometer input, (*b*) 6BC5 input, (*c*) Feedback circuit. Circuit (*a*) or (*b*) connects with circuit (*c*).

little adjustment after initial calibration. It is useful in the mid audiofrequencies where the transformer introduces little phase shift. The second circuit uses transistors (Fig. 3 *b*) and is adequate from zero to 25 kc. The output, however, must be balanced and checked as the transistors and battery voltages change with time. Both circuits include provision for nulling D.C. voltage changes. Over-all sensitivity is 0.02 megohm over the range of 0 to 5 megohms for impedance magnitude measurements and one-half degree for the phase angle.

D.C. voltage changes can also be measured by inserting the D.C. comparison or compensating voltage in series with the ground return. This method is preferred especially when recording A.C. impedances at input voltages other than zero. Shifting the dynamic operating point of the input amplifier introduces phase shifts of several degrees in the measured A.C. impedance at the higher frequencies. Therefore A.C.

impedances are measured at zero input voltage by inserting the compensating D.C. voltage in series with the ground return.

The input amplifier is one of two similar types. An input cathode follower has its power supply driven by a unity gain amplifier (Fig. 4). Either a C.K. 5886 electrometer tube, grid current 10^{-14} amp (Fig. 4 *a*), or a selected 6BC5, grid current 10^{-11} amp. (Fig. 4 *b*), is used. A feedback loop provides for unity gain and for input capacity compensation (Fig. 4 *c*). The input capacities for circuits 4*a* and 4*b* are 0.3 $\mu\mu$f and 0.1 $\mu\mu$f, respectively. With capacitance compensation lower figures are obtainable. In practice, connection of a calomel or Ag–AgCl cell and micropipette to the input grid usually increases the input capacitance to 2 to 5 $\mu\mu$f. Ag–AgCl cells are usually used since smaller input capacities are obtained than with larger calomel cells.

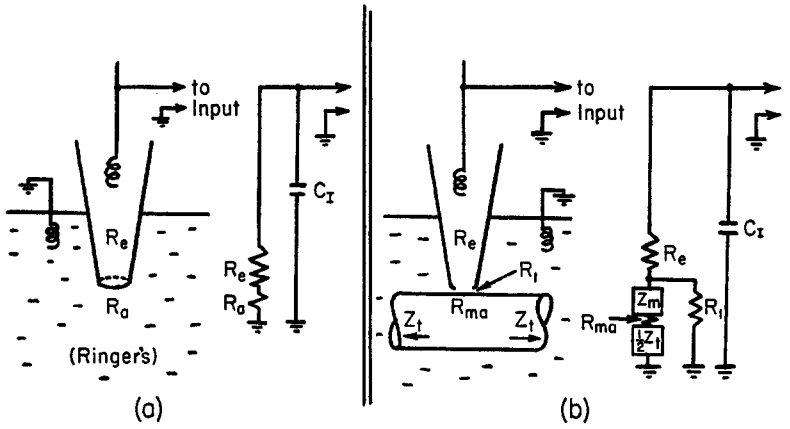

FIGURE 5. Input electrical circuits. (*a*) Input circuit before contacting muscle surface. (*b*) Input circuit after contacting muscle surface. R_e, electrode resistance, R_a, pipette tip access resistance, R_I, leakage resistance, R_{ma}, membrane access resistance, Z_m, membrane impedance, Z_t, transmission line impedance of muscle, C_I, input capacity.

The apparatus is mounted in a cage electronically driven with the headstage power supply (Fig. 4 *c*). Driven shields around the input grid are not used as they increase input capacity. The micromanipulator and other metal parts are not grounded but driven as the cage. The muscle chamber is plastic and when possible nylon screws are used. The headstage tube is mounted on a siliconized plastic mount. The wire from the input grid to the Ag–AgCl electrode in the pipette is under 3 cm long and small (32 gauge). The Ringer pool is kept small and the pipettes are about 2 cm long with siliconized shanks. These provisions reduce stray input capacity.

Transistorizing the rectangular wave voltage generator avoids A.C. pickup. Voltage outputs up to 90 volts are obtainable with a rise time of 4 microseconds, 95 per cent complete in 6. The oscillator is a Hewlett Packard No. 200 CD, the oscilloscope a dual beam tektronix model 502, modified to allow variable gain in the vertical amplifiers. Temperature is measured by a thermistor.

D. *Measuring Technique and Theory*

With its tip in Ringer solution the D.C. resistance of the electrode, R_e, in series with the access resistance, R_a, is determined by recording the voltage drop due to passage of a known current (Fig. 5 *a*). The A.C. impedance is calibrated against the D.C. resistance by adjusting the coupling condenser, usually at 500 cycles where the impedance is mostly resistive with phase angles under 1°. Resistances of 0.5 to 2 megohms are usual for Ringer-filled pipettes with tips of 20 to 10 microns.

The electrode tip is positioned a tenth of a millimeter or less above the muscle and the Ringer solution is lowered to a millimeter or less above it. Measurements are made at 500 cycles to 25 kc, and the impedance locus is plotted to determine amplifier input capacitance C_i, and to verify the use of lumped values R_e, and C_i, to represent electrode resistance and input capacitance. Lumped representation of R_e and C_i appears justified, because impedance loci of the electrodes appear as segments of near perfect semicircles with little internal phase angle, and the pipettes used have rapidly converging tapers. A tip taper of large solid angle can localize all but a few per cent of the electrode resistance within the first hundred microns or less of the tip. Similarly, calculations and electrolytic tank studies place most of the tip access resistance R_a in a region of 5 to 10 tip diameters. Capacity distribution is minimum at the amplifier input and maximum in the Ringer solution bath. In pulling down glass tubing, diameter ratios tend to remain constant (Stuetzer, 1950). For an outside to inside diameter ratio of 2:1.5 the distributed capacity for a pipette tip in Ringer solution is calculated as 7.0 $\mu\mu$f/cm. Little phase shifting is therefore expected at the low frequencies used if 0.07 $\mu\mu$f is distributed along 100 microns of a pipette resistance of 1 megohm. Impedance measurements with long taper electrodes show flattened and distorted circle diagrams with reductions in reactance amounting occasionally to 50 per cent. For such electrodes, a lumped representation of pipette resistance and input capacitance is not justified and perfect input capacity compensation is not possible. Impaling microelectrodes, filled with 3 M KCl and immersed in Ringer solution, show little internal phase angle for the impedance locus provided the tip taper is rapid and not tapered as described by Ling and Gerard (1949).

Since most electrodes behave nearly ideally with respect to their impedance loci, the amplifier input capacitance C_i is calculated from the relationship $\tan \theta = wRC_i$ where θ = impedance phase angle; $w = 2\pi f$, where f = frequency (cycles/sec.); and $R = R_e + R_a$, the electrode plus access resistance. Ordinarily, input capacitive compensation is not used because it introduces errors into the impedance measurements.

Rectification is next examined for by passing current pulses up to 4.5×10^{-7} amp through the Ag–AgCl electrodes and pipette. Ordinarily no rectification is detected for the Ag–AgCl electrodes and for the pipette tips.

After $R_e + R_a$, and C_i have been determined the electrode is applied to the muscle surface with less than 100 microns additional movement, since greater displacement changes input capacitance. Upon contact the impedance increases. The idealized input circuit is diagrammed in Fig. 5 *b*. If the contribution of C_i is subtracted the impedance of Fig. 5 *b* plots as a semicircle in the complex impedance plane. The D.C. and low frequency intercept with the real axis is at $R_e + R_1$ and the infinite

frequency intercept is approximately at R_e + (R_1 paralleled with R_{ma}). The relative impedance contributions will now be considered.

The pipette resistance, R_e, is obtained by subtracting pipette access resistance, R_a, from $R_e + R_a$ (Fig. 6 *a*). R_a is usually only a few per cent of R_e, and measurements with electrolytic tank models show it to vary about 25 per cent with the tip geometries encountered. Access resistance is taken as $R_a = r/5a$ where r = resistivity of the bath solution and a = the inside tip radius. This compares with the access resistance to one side of a disc calculated as $r/4a$ (Jeans, 1958). Typically R_1 is one or more times R_e.

If C_m = 3 μf/cm² and R_m = 1 to 2 × 10³ ohm cm² (Katz, 1948), the resting membrane impedance is primarily capacitive at frequencies over 500 cycles per second. The resting resistance of the delimited membrane region is ordinarily much greater than the leakage resistance and as a parallel circuit element can be ignored. During activity, however, the membrane resistance may contribute to the measured impedance.

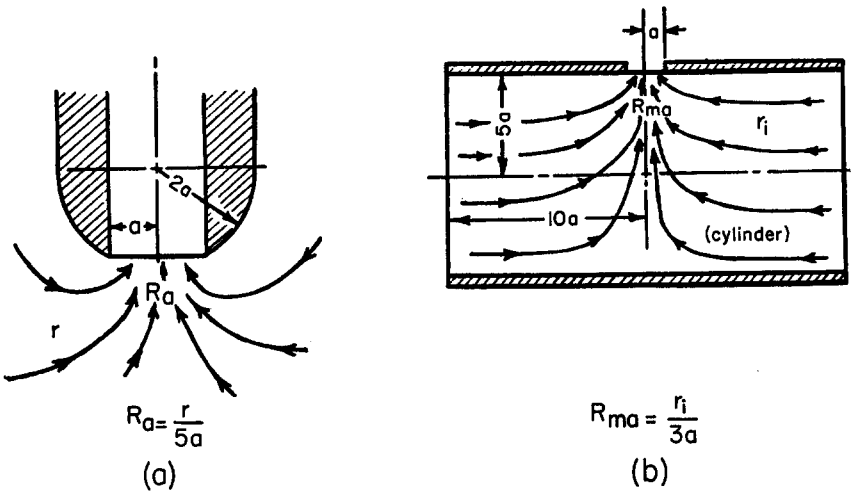

FIGURE 6. Electrolytic tank measurements of access resistances. (*a*) Pipette tip access resistance R_a. (*b*) Membrane access resistance R_{ma}. r, resistivity of solution (ohm cm). a, radius of pipette tip (cm).

The membrane access resistance, R_{ma}, is estimated from a tank model (Fig. 6 *b*). Shortening the model by half lowers the access resistance about 10 per cent indicating that most of the membrane access resistance lies within a hemisphere of 5 tip diameters. The model experiments give $R_{ma} = r_i/3a$ where r_i = sarcoplasm resistivity and a = pipette tip radius. In the muscle fiber, shunting of R_{ma} by the membrane occurs at higher frequencies. At infinite frequency the membrane impedance is zero and the membrane access resistance is close to $R_{ma} = r_i/5a$ since most of the access resistance is in sarcoplasm and part in the Ringer solution.

The characteristic impedance, Z_t, of a transmission line or core conductor for

continuous A.C. current is (King, Minno, and Wing, 1945):

$$Z_t = \left[\frac{r_i}{2\pi^2 a^3}\left(\frac{1}{1/r_m^2 + w^2 C_m^2}\right)^{\frac{1}{2}}\right]^{\frac{1}{2}}$$

$$\text{Tan } (2\theta) = -wr_m C_m$$

where r_i = specific sarcoplasm resistivity (ohm cm); r_m = specific membrane resistance (ohm cm²); C_m = specific membrane capacity (farads/cm²); a = muscle fiber radius (cm); $w = 2\pi f$; where f = frequency (cycles/sec.); θ = phase angle (degrees). For D.C. this reduces to $Z_t = (r_i r_m/2\pi^2 a^3)^{\frac{1}{2}}$. These expressions for an infinite transmission line also hold when the fiber length is several length constants and when one can neglect end reflections (Weidman, 1952). For the frog sartorius muscle the length constant ranges from 0.55 mm to 0.85 mm (Katz, 1948). Therefore, the above expression for Z_t is used since measurements are taken near the midregion of the muscle whose fibers are many length constants long.

Since two transmission line impedances are in the return path to ground the impedance contribution is $Z_t/2$. The total impedance paralleling the leakage resistance R_1 may be written as $Z_m + R_{ma} + Z_t/2$.

To evaluate the relative contributions of the above impedances consider a muscle fiber of 80 microns diameter, r_m = 1000 ohm cm², r_i = 400 ohm cm (7°C, Strickholm, 1957), $C_m = 3 \times 10^{-6}$ f/cm², and pipette tip diameter = 20 microns. For a resting membrane, the absolute impedances at D.C. have the following ratio in megohms: $Z_m : R_{ma} : Z_t/2$ = 318:0.13:0.33. At 500 cycles the ratio is 33:0.13:0.07 and at 5 kc the ratio is 3:0.13:0.02. If the membrane resistance decreases during activity to $\frac{1}{100}$ of its resting value, the absolute value of Z_m for D.C., 500 cycles, and 5 kc, becomes 3.2, 3.1, and 2.3 megohms respectively. Therefore, at lower frequencies the membrane impedance is the major element paralleling R_1. At higher frequencies both Z_m and Z_t vanish leaving R_{ma} in parallel with R_1. The effect of Z_t, which is complex, and of R_{ma} is to distort the impedance circle diagram and to displace the infinite frequency intercept of the impedance locus with the real axis. The effects are usually small.

It is assumed above that the voltage at the surface of the examined region is uniform, and that the leakage resistance, R_1, is constant and resistive without being shunted by the membrane over the frequencies used. The immediately subjacent, intracellular voltage may be considered relatively uniform for the frequencies at which membrane impedance is much greater than that of the membrane access and transmission line impedances. The voltage distribution at the cell surface under a pipette tip is obtainable from tank models. The model geometry of Fig. 7 is considered representative. Similar model measurements have been made by Huxley and Taylor (1958).

Electron microscopy shows the muscle surface to contain outer (250 to 300 A), possibly mucoprotein, and inner (75 A), limiting, osmiophilic layers (Porter and Palade, 1957; Cedergren, 1959; Robertson, 1959, 1958), surrounded by two classes of fibrils one of less than 100 A and one between 250 to 350 A diameter (Robertson, 1956; Porter and Palade, 1957). If the resistive membrane is at the inner layer, then the thickness of the leakage resistance layer could be under 600 A with an effective

thickness much less if the material in the resistance layer is non-conductive. As the contact pressure of a pipette against the cell surface increases, the increase in leakage resistance R_1 diminishes and R_1 appears limited. This suggests that contact spacing between the pipette tip and cell surface is limited by the nature of the muscle cell surface. Experiments utilizing selected pipette tips whose shape limits the maximum leakage path length, and with moderate contact pressure, indicate an equivalent clear channel spacing of 200 A for a 20 micron diameter pipette having a 1 megohm leakage path of length not over 1 micron. Measurements with micropipettes inserted within the surface-applied pipettes indicate uniformity of voltage at the cell surface when voltages are applied to the interior of the surface-applied pipettes. Similar measurements with impaling micropipettes, inserted into the muscle fiber and beneath the delimited membrane region, detect no change in intracellular voltage when

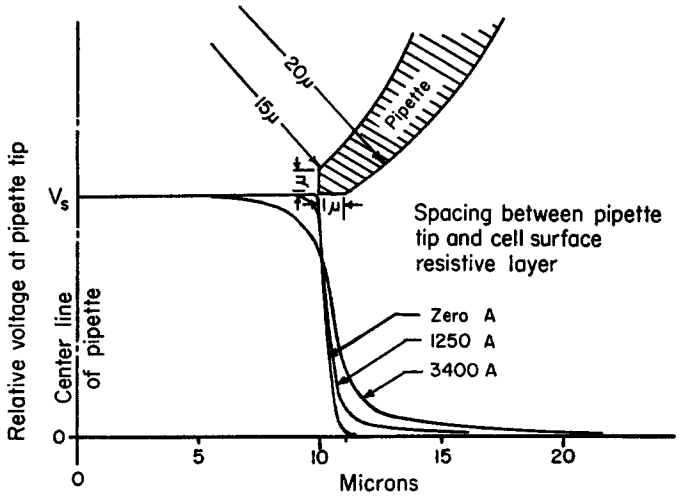

FIGURE 7. Voltage profile at pipette tip against muscle cell surface.

non-excitatory voltages are applied to the interior of the surface-applied pipettes. In addition, micropipettes placed external to the cell surface and immediately adjacent to the surface-applied pipette tips detect no external spread of voltage. These experiments indicate that although variations in leakage path length and thickness undoubtedly exist, these variations have little effect on the uniformity of voltage across the delimited membrane region and in addition indicate that the voltage drop from the delimited region to the external bath solution is almost entirely across the leakage resistance path. This result is that theoretically expected if the equivalent leakage path thickness averages 200 A (Fig. 7). Therefore the impedance of the delimited membrane region and the leakage resistance path may be mathematically treated separately.

Transmembrane resistance and capacity are distributed along the leakage path. The geometry of the leakage resistance and membrane shunt permit it to be approximated as a transmission line terminated in a portion of the membrane access resistance

in series with one-half the transmission line impedance of the muscle fiber, provided the leakage resistance path length is much less than the pipette diameter. For typical values (20 micron tip diameter, $R_1 = 10^6$ ohms of 1 micron path length, $C_m = 3$ $\mu f/cm^2$, $R_m = 10^3$ ohms/cm^2), R_1 is primarily real with a phase angle of $-7°$ at $w = 2\pi f = 10^5$ (where f = frequency). If the muscle membrane under the leakage resistance path undergoes activity with a 100-fold resistive drop, the leakage resistance changes little in phase angle and in magnitude at $w = 10^5$. At zero frequency or D.C., a similar membrane change alters leakage resistance less than 1 per cent. Therefore at frequencies probably up to 5 kc, R_1 is primarily resistive and constant in magnitude during rest and activity.

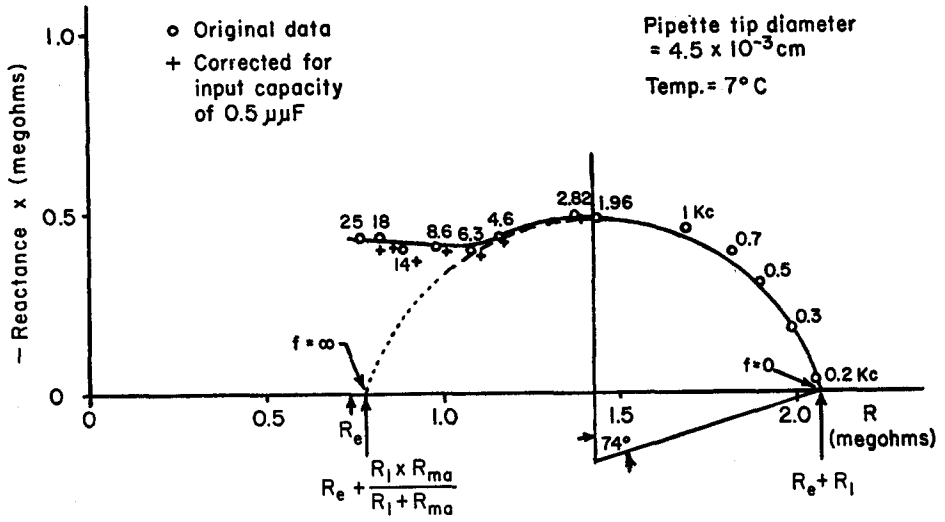

FIGURE 8. Impedance locus of resting muscle membrane. Experiment 6. Dashed line is extrapolation of impedance locus to infinite frequency. Impedance points at higher frequencies include an undetermined phase shift error introduced by utilizing some input capacity compensation.

Thus, for a membrane behaving as a parallel resistive and capacitive element, the impedance locus (Fig. 5 *b*) in the valid range will be a semicircle after subtraction of input capacity. At zero frequency the impedance locus intercepts the real axis at $R_e + R_1$ and the infinite frequency intercept is at $R_e +$ (R_1 paralleled with R_{ma}), assuming zero membrane impedance at infinite frequency. This is also true if the membrane capacity behaves as a polarization element (Cole, 1933) where the capacity acts as if it has a series resistive element, the combination having a phase angle independent of frequency. From the impedance diagram an equivalent membrane capacity may be calculated. Since the leakage resistance R_1 is much less than the resting membrane resistance R_m, no information about R_m is obtainable. However, if during membrane activity, R_m contributes to the impedance locus, an equivalent value for membrane resistance and capacity can be calculated. Caution, however,

must be exercised in interpreting these membrane equivalent resistances and capacitances with physical counterparts.

Few impedance measurements are taken above 20 kc because of uncertainties in considering R_1 as a real resistance. Also errors in the input capacity make analysis difficult especially for small regions whose total capacity is near that of the amplifier input. At the lower frequencies satisfactory analysis is possible and is done most simply by graphical vector methods.

TABLE I

No.	Pipette Tip diameter	R_e	R_1	T	Phase angle of impedance locus	Phase angle of membrane capacity at 5 kc.	Equivalent membrane capacity at 5 kc.
	microns	*megohms*	*megohms*	*°C*	*degrees*	*degrees*	*μf/cm²*
1	20	0.67	1.89	7	72	81	2.9
2	20	0.57	2.13	20	78	78	5.4
3	20	0.70	1.60	20	76	73	6.3
4	45	0.44	0.64	7	67	68	6.9
5	45	0.44	0.72	7	70	69	3.7
6	45	0.74	1.31	7	74	73	2.8
7	17	1.37	1.79	7	78	79	3.3
8	22	0.89	1.51	7	73	65	2.0
9	22	0.27	0.90	7	72	51	5.1
10	29	0.23	0.70	7	76	67	1.5
11	29	0.23	0.92	7	74	73	1.9
12	27	0.29	0.92	9	72	69	2.0
13	27	0.30	0.75	9	70	73	1.8
14	29	0.23	0.69	6	70	70	3.7
Average					73	71	3.5

RESULTS

A 45 micron tip pipette, used to minimize input capacity errors and to obtain measurements in the lower frequency range, was placed against a muscle cell and yielded the complex plane impedance plot shown in Fig. 8. The dashed curve of Fig. 8 shows the impedance locus after subtraction of a measured input capacity of 0.5 $\mu\mu$f. At the low frequencies the impedance plot intersects the real axis at $R_e + R_1$. At high frequencies, after input capacitance subtraction, it extrapolates to R_e plus the parallel resistance of R_1 and R_{ma} as an intercept. An internal phase angle of 74° appears which need not imply a complex or frequency-dependent membrane capacitance, since the membrane access resistance R_{ma} and transmission line impedances $Z_t/2$ are in series with the membrane capacity C_m. If R_{ma} is assumed to be resistive its only effect in series with C_m would be to displace the high frequency intercept of the impedance locus and reduce the size of the curve without changing the internal

phase angle. The transmission line impedance is, however, complex and its effect, which would distort the impedance locus, must be considered. If values are assumed which would give an unfavorably large value for transmission line impedance ($r_m = 10^4$ ohm cm^2, $r_i = 400$ ohm cm at 7°C, $C_m = 3 \times 10^{-6}$ f/cm^2, and fiber diameter = 50 microns), then at 2.82 kc, $Z_t/2 = 0.07 \times 10^6$ ohms with a phase angle $\theta = -45°$. This is insufficient to account for the observed phase angle.

Therefore, the transmission line impedance probably cannot account for the depression of the impedance diagram. A possible cause is the complex leakage path resistance. From the data of Fig. 8, a leakage resistance with phase angle under 1° is estimated for 2.82 kc. Therefore, the membrane capacitor seems to behave not as a pure capacitance but as a complex element representable at 2.82 kc by a capacity of 3.1 μf/cm^2 and a series resistance of 5.7 ohm cm^2. The impedance locus internal phase angle is 74°. Other experiments (Table I) also indicate a complex membrane capacitance.

DISCUSSION

A number of theories concerning a depressed impedance locus diagram with an internal phase angle have been reviewed elsewhere (Schwann, 1957). Several points merit emphasis.

Table I shows internal phase angles averaging (73°), only a few degrees higher than those obtained by other authors (Bozler and Cole, 1935, 70°; Cole and Curtis, 1936, 71°; Guttman, 1939, 70 to 71°; Schwann, 1957, 66 to 75°). It is of interest that the present method yields results comparable to those obtained by others with very different techniques. The depressed impedance locus could result from a polarization type capacity which is describable mathematically by assuming a frequency-dependent membrane capacity whose phase angle is constant (Cole and Cole, 1941). Hence, for muscle, membrane capacity ranges from 1 μf/cm^2 at high frequencies to 20 μf/cm^2 at 10 cycles/sec. (Schwann, 1957). Plots of $\log [(Z-Z_\infty)/(Z_0-Z)]$ against $\log f$, which would plot as a straight line for a polarization type capacity, have not been of sufficient absolute accuracy to determine whether this is the case.

An internal phase angle, when whole muscle is used, could also result from a statistical distribution of fiber diameters and membrane capacities as well as other mechanisms (Cole and Curtis, 1936). In the present experiments, however, measurements have been made on a small region of a single muscle fiber. Therefore, fiber multiplicity cannot be responsible. A comparable explanation, however, might hold that the depression of the impedance locus results from a microscopic distribution function of capacitors in series with resistors. An infinite number of frequency-independent capacitors with resistors in

series could account for the results (Schwann, 1957). The cell membrane, if it resides in the complex layer of lipoproteins at the cell surface is undoubtedly not homogeneous, and probably continually undergoes microlocal variations in thickness, dielectric constants, and in microaccess resistances (Tobias, 1959).

Another explanation for a frequency-dependent membrane capacity has been that relaxation phenomena could occur in ionic atmospheres or in an electric double layer at the cell surface. There is evidence that this probably occurs in fat emulsions and with small polystyrene spheres (Schwann, 1957). Depression of the impedance circle diagram also occurs with the polarization layer at metal-solution interfaces, (Cole, 1933) and electric double layers on biological membranes could possibly behave similarly. Polar orientation of molecules may also be involved in producing the observed results. In this respect, any mechanism which produces a time or phase difference between impressed voltage and charge displacement or current will appear as a complex impedance element (Teorell, 1953). Pure membrane capacitive and resistive terms if combined with any of the above mechanisms could appear in impedance analysis as frequency-dependent elements. It may be that at high frequencies the measured capacity of 1 $\mu f/cm^2$ is representative of relatively fixed membrane structure while the increase in capacity observed at lower frequencies involves other phenomena. Interpretation of capacitance measurements at lower frequencies in biological media, therefore, requires caution, especially when impedance changes during membrane activity are involved. A resting membrane capacity of 40 $\mu f/cm^2$ has been measured for crustacean muscle (Fatt and Katz, 1953). This could, as described by the authors, result from a high degree of membrane folding but other interpretations are possible.

The author wishes to thank Dr. Julian Tobias for critical discussion of the above work. He is also grateful to the many people at the University of Chicago who generously lent some of the equipment. This work has been supported in part by a grant from the United States Public Health Service and in part by a grant from the Dr. Wallace C. and Clara A. Abbott Memorial Fund of the University of Chicago. It was submitted to the Department of Physiology, University of Chicago, in partial fulfillment of the requirements for the degree, Doctor of Philosophy.
Received for publication, August 18, 1960.

BIBLIOGRAPHY

BOZLER, E., and COLE, K. S., 1953, Electric impedance and phase angle of muscle in rigor, *J. Cell and Comp. Physiol.* **6**, 229.

CEDERGREN, EBBA-ANDERSSON, 1959, Ultrastructure of motor end plate and sarcoplasmic components of mouse skeletal muscle as revealed by three dimensional reconstructions from serial sections, *J. Ultrastructure Research*, suppl. 1.

COLE, K. S., 1932, Electric phase angle of cell membranes, *J. Gen. Physiol.*, **15**, 641.

COLE, K. S., 1933, Electric conductance of biological systems, *Cold Spring Harbor Symp. Quant. Biol.*, **1**, 107.

COLE, K. S., and COLE, R. H., 1941, Dispersion and absorption in dielectrics, *J. Chem. Physics*, **9**, 341.

COLE, K. S., and CURTIS, H. J., 1936, Electric impedance of nerve and muscle, *Cold Spring Harbor Symp. Quant. Biol.*, **4**, 73.

FATT, P., and KATZ, B., 1953, The electrical properties of crustacean muscle fibers, *J. Physiol.*, **120**, 171.

GELFAN, S., 1930, Studies of single muscle fibers. I. The all or none principle, *Am. J. Physiol.*, **93**, 1.

GELFAN, S., and GERARD, R. W., 1930, Studies of single muscle fibers. II. A further analysis of the grading mechanism, *Am. J. Physiol.*, **95**, 412.

GUTTMAN, R., 1939, The electrical impedance of muscle during the action of narcotics and other agents, *J. Gen. Physiol.*, **22**, 567.

HUXLEY, A. F., and TAYLOR, R. E., 1958, Local activation of striated muscle fibers, *J. Physiol.*, **144**, 426.

JEANS, J. H., 1958, The Mathematical Theory of Electricity and Magnetism, Cambridge University Press, 352.

KATZ, B., 1948, The electrical properties of the muscle fiber membrane, *Proc. Roy. Soc. London, Series B*, **135**, 506.

KING, R., MINNO, H., and WING, A., 1945, Transmission Lines, Antennas, and Wave Guides, New York, McGraw Hill Publishing Co., Inc.

LING, G., and GERARD, R. W., 1949, The normal membrane potential of frog sartorius fibers, *J. Cell. and Comp. Physiol.*, **34**, 383, 396.

PLATEAU, F., 1917, *in* On Growth and Form, Thompson, Sir D'arcy Wentworth, Cambridge University Press, 220.

PORTER, K. R., and PALADE, G. E., 1957, Studies on the endoplasmic reticulum, *J. Biophysic. and Biochem. Cytol.*, **3**, 269.

PRATT, F. H., 1930, On the grading mechanism of muscle, *Am. J. Physiol.*, **93**, 9.

PRATT, F. H., and EISENBERGER, J. P., 1919, The quantal phenomena in muscle, *Am. J. Physiol.*, **49**, 1.

ROBERTSON, J. D., 1956, Some features of the ultrastructure of reptilian skeletal muscle, *J. Biophysic. and Biochem. Cytol.*, **2**, 369.

ROBERTSON, J. D., 1958, The cell membrane concept, *J. Physiol.*, **140**, 58P.

ROBERTSON, J. D., 1959, The ultrastructure of cell membranes and their derivatives, *Biochem. Soc. Symp.*, **16**, 1.

SCHWANN, H. P., 1957, Electrical properties of tissue and cell suspensions, *Adv. Biol. and Med. Physics*, **5**, 147.

STEINMAN, S. E. 1937, Factors determining the type of response in the fiber of striated muscle, *Am. J. Physiol.*, **118**, 492.

STRICKHOLM, A., 1957, The absolute electrical conductivity of amphibian muscle determined by impedance measurements utilizing a single exploring micro-electrode, *Tr. Biophysic. Soc.*, **1**, in press.

STRICKHOLM, A., 1960, The absence of a sodium equilibrium potential in excitation currents of a small isolated region of a frog muscle membrane, *Fed. Proc.*, **19**, in press.

STUETZER, O. M., 1950, Microspacer electrode technique, *Proc. IRE*, **38**, 871.

TAYLOR, C. V., 1925, Microelectrodes and micromagnets, *Proc. Soc. Exp. Biol. and Med.* **23**, 147.

TEORELL, T., 1953, Transport processes and electrical phenomena in ionic membranes, *Progr. Biophysic. and Biophysic. Chem.*, **3**, 305.

TOBIAS, J. M., 1959, Biophysical aspects of conduction and transmission in the nervous system, *Ann. Rev. Physiol.*, **21**, 299.

WEIDMAN, S., 1952, The electrical constants of Purkinje fibers, *J. Physiol.*, **118**, 348.